Applied Catalysis B: Environmental 250 (2019) 355–368

Contents lists available at ScienceDirect

Applied Catalysis B: Environmental

journal homepage: www.elsevier.com/locate/apcatb

Influence of Na, P and (Na + P) poisoning on a model copper-ferrierite NH_3-SCR catalyst

Marie-Laure Tarot[a], Eduard Emil Iojoiu[b], Vincent Lauga[b], Daniel Duprez[a], Xavier Courtois[a,*], Fabien Can[a,*]

[a] University of Poitiers, CNRS, UMR 7285 Institut de Chimie des Milieux et Matériaux de Poitiers (IC2MP), 4 rue Michel Brunet – TSA 51106, 86073 Cedex 9, France
[b] Renault Trucks – Volvo Group Trucks Technology – Powertrain Engineering Lyon, 99 route de Lyon, 69806 Saint-Priest Cedex, France

ARTICLE INFO

Keywords:
NOx-NH_3-SCR
Sodium
Phosphorus
Copper exchanged zeolite
Deactivation

ABSTRACT

To highlight the deactivation mechanisms encountered by minerals impurities from biodiesel, the effects caused by Na, P or (Na + P) additions were studied over a model Cu-FER catalyst. Na, P or (Na + P) were added by wet-impregnation in water in a wide concentration range up to 2 wt-%. The catalytic behaviors were evaluated by NH_3/NO oxidation and standard/fast NH_3-SCR reactions. In addition, a combination of several characterization techniques (ICP–AES, N_2 adsorption/desorption, XRD, NH_3-TPD, NO adsorption monitored by FTIR and H_2-TPR) was applied to provide useful information regarding the deactivation mechanism caused by the minerals addition. Sodium and phosphorus interacted differently with the Cu-FER catalyst. Na addition induced a loss of Brønsted acid sites and a back-exchange of Cu^{2+} with Na^+, with formation of external CuO species, thus favoring the oxidation of NO and NH_3. After phosphorus addition, the exchanged Cu^{2+} species remained moderately affected, but direct interactions with copper were evidenced which were primarily responsible for catalyst deactivation toward the oxidation reactions. After equimolar addition of phosphorus and sodium, both Na and P effects were observed. For the NH_3-SCR process, the ammonia adsorption ability, which depends on both acidity and copper units, appeared the main key parameter driving the catalytic activity at low temperature ($T \leq 250\,^{\circ}C$). Phosphorus appeared to be the major responsible for catalyst deactivation after (Na + P) co-poisoning.

1. Introduction

The NH_3-SCR process is commonly used worldwide to respect the highest current standards like Euro 6/VI related to NOx emission of passenger cars and heavy duty vehicles. The main involved reactions are the “standard-SCR” reaction (Eq. (1)) and the “fast-SCR” reaction (Eq. (2)).

$$2NH_3 + 2NO + \tfrac{1}{2}O_2 \rightarrow 2N_2 + 3H_2O \quad (1)$$

$$2NH_3 + NO + NO_2 \rightarrow 2N_2 + 3H_2O \quad (2)$$

The NH_3-SCR technology was initially developed to control nitrogen oxides emissions from power plants and stationary source. The dedicated catalysts are then V_2O_5-WO_3-TiO_2 based materials. With the adjustment of this process to the treatment of automotive exhaust gas, new catalytic formulations have emerged to expand the operating temperature, to prevent the deactivation due to transition phase of TiO_2 (from anatase to rutile, responsible for the high temperature deactivation) and to overcome the problem of vanadium sublimation. Subsequently, numerous efforts were made to replace vanadium-based SCR catalysts with new generations of metal-exchanged zeolite-based systems. For this purpose, a large variety of zeolites have been proposed (ZSM-5, mordenite, beta, ferrierite, Y-zeolite, chabazite, …) and Cu-promoted catalysts based on small pore zeolites are commonly used to ensure low-temperature DeNOx activity and high resistance to thermal aging. Reaction mechanism of the NH_3-SCR process over Cu-exchanged zeolite catalysts has been studied in numerous works [1]. Briefly, Cu-zeolite based catalysts have two kinds of active sites. Acid sites are provided by the zeolite framework to adsorb and activate ammonia while Cu species ($[Cu^{2+}-OH^-]^+$, Cu–O–Cu or Cu^+ species) provide redox sites involved in the catalytic cycle of the NOx reduction into N_2. High DeNOx catalytic performances are achieved by a well balance between acid and redox sites. For instance, a high Cu loading induces an over consumption of the reducer caused by ammonia oxidation which is detrimental to the DeNOx efficiency at high temperature. However, the exact nature of appropriate Cu species is not well

* Corresponding authors.
E-mail addresses: xavier.courtois@univ-poitiers.fr (X. Courtois), fabien.can@univ-poitiers.fr (F. Can).

https://doi.org/10.1016/j.apcatb.2019.03.044
Received 12 September 2018; Received in revised form 14 February 2019; Accepted 16 March 2019
Available online 18 March 2019
0926-3373/

understood. It is proposed that the Cu atoms can be coordinated to the oxygen atoms in Si–O–Al bridges to probably form solvated $[Cu^{2+}-OH^{-}]^{+}$ unit, balanced by one framework negative charge and Cu^{2+} species balanced by two nearby framework negative charges, commonly abbreviated as Cu^{2+}-2Z and $[Cu(OH)]^{+}$-Z, where Z represents a charged zeolite framework site [2–4]. Additionally, $(Cu^{2+}-O^{2-}-Cu^{2+})^{2+}$ dimers can be formed by the combination of $[Cu^{2+}-OH^{-}]^{+}$ or Cu^{+} species [5]. The SCR reaction mechanism is associated to a redox cycle in which the reduction part corresponds to the N_2 formation by NH_3-NOx reaction and the oxidation part is related to the re-oxidation of the catalytic site and the activation of NO. During the reduction part, Cu^{2+} is reduced into Cu^{+}. Recently Janssens *et al.* [6], have proposed that the re-oxidation of Cu^{+} involves the oxidation of NO to recover the catalytic site. Thereafter, as proposed in many work, the activation and oxidation of NO to NO_2 is a key step of the SCR mechanism [7].

In addition to pollutant emissions regulations, the European states have made pledges to reduce the carbon impact of vehicles, especially toward the CO_2 emission. Biodiesel is also a promising renewable fuel to limit the dependence on usual fossil fuels. For this purpose, European Directive 2009/33/CE imposes a minimal concentration of biodiesel in the commercialized diesel fuel. However, biodiesel contains mineral traces such as sodium, potassium or phosphorus, which are authorized in limited amounts (maximum of 5 and 4 ppm for Na + K and P, respectively, in European Union; EN 14214). Nevertheless, the intensive use of biodiesel as encountered for some captive fleets can induce detrimental effects to the whole catalytic after-treatment systems by means of mineral deposits, as recently reported [8]. It was demonstrated in particular that DOC poisoning was very disadvantageous to the SCR efficiency because of the deactivation in the NO oxidation into NO_2. When both DOC and SCR were poisoned, high deactivation was recorded.

Few studies relate the deactivation mechanism of poisoned exchanged-based zeolite by alkalies (Na, K) or phosphorus (P). The deactivation of P-containing zeolite-based samples exposed to phosphoric acid was evidenced for instance by Shwan et al. [9] (Fe-BEA), Andonova et al. [10] (Cu-BEA) and Xie et al. [11] (Cu-SSZ-13). The main conclusion was a significant decrease in the DeNOx activity at low temperature (T < 300 °C) over iron-exchanged zeolite, by means of formation of metaphosphates species (PO_3^{-}) that replace hydroxyl groups on the active iron species in Fe-BEA. The strong deactivation of P-containing Fe-BEA zeolite was also confirmed in [12], attributed to an unclear direct interaction of phosphates with the active Fe-species. Concerning Cu-BEA, the overall deactivation was found to occur mostly by chemical deactivation reducing the number of active Cu species, deteriorating the redox properties of the P-containing copper-exchanged catalysts. Additionally, sodium and potassium also lead to deactivation. Exposition of a Fe-BEA zeolite to an aqueous solution of KNO_3 results in a decrease in the Brønsted acidity and in a loss of active isolated iron species [13]. An increase in both the NOx storage behaviour and the NO oxidation activity was also evidenced. Similar tendencies were observed on Cu-SAPO-34 [14] and Cu-SSZ-13 [15] after sodium addition by incipient wetness impregnation. Ma et al. [14] also noticed that the standard-SCR activity is not impacted with 0.5 wt-% of potassium. Recently, we studied the effect of the sodium addition mode on model Cu-FER SCR catalysts with two copper loadings (2.8 wt-% and 6.1 wt-%), in order to compare samples with or without over exchanged copper [16]. Na was added by wet-impregnation using two solvents, namely water or ethanol. Acidic sites concentration was strongly decreased by Na additions, concomitantly with a migration of the Cu exchanged species leading to the formation of external CuO compounds. This latest Cu^{2+}-Na^{+} back exchange was found to be especially favored when the deposition of Na was performed in an aqueous solvent. It results that Na impregnation in water led to a stronger catalyst deactivation than impregnation in ethanol.

The aim of this work is to investigate the more realistic simultaneous (Na + P) addition on an exchanged copper-ferrierite (Cu-FER) model SCR catalyst. Firstly, the deactivation mechanism caused by phosphorus (P) addition alone have to be examined and compared with that encountered after single alkali (Na) element deposition. Results are then compared with the (Na + P) combination to highlight the role of each poison in the NH_3-SCR reactivity. Based on the SCR mechanism, a special attention is paid on ammonia and NO adsorption/oxidation behaviors toward Cu-FER, together with the NH_3-SCR performances.

2. Experimental part

2.1. Catalysts preparation

A FER zeolite (ferrierite ammonium zeolite, SiO_2/Al_2O_3 = 20, Alfa Aesar), which exhibits a channel system of 10 and 8 member rings, was selected to ensure a high hydrothermal stability. In order to obtain a catalyst with predominantly copper in the exchange position, a sample with 2.8 wt-% of Cu (measured by ICP elemental analysis) was prepared as previously reported in [16]. Copper was added using the ion exchange method with 10 g of zeolite in suspension in $Cu(CH_3COO)_2$ (Aldrich) diluted in ultra-pure water. The pH was adjusted at 5 with HNO_3 to prevent the zeolite dealumination and the hydroxide copper formation, based on the diagram of copper speciation from Ajmal et al. [17]. The solution was stirred under reflux at 80 °C for 23 h. Solution was then filtered and thoroughly washed with ultra-pure water and dried at 120 °C for 15 h. The resulting powder was firstly treated 30 min at 600 °C under 10% O_2-90% N_2 (heating rate: 2 °C min^{-1}). Vapour water (10%) was then added and the catalyst was maintained at 600 °C for 16 h before cooling to room temperature. The corresponding stabilized sample is denoted Cu-FER.

The considered inorganic elements (Na, P and Na + P) addition were made by impregnation: 1.5 g of the catalyst was suspended in 4 mL of water with the desired amounts of sodium (from $NaNO_3$ salt), phosphorus (from $(NH_4)_2HPO_4$ salt), or sodium and phosphorus in equimolar contents (from H_2NaPO_4 salt). The solution was then stirred at room temperature during 4 h. After solvent evaporation, the sample was dried one night at 80 °C. Finally, the resulting powder was submitted to a thermal treatment composed of 30 min at 600 °C under 10% O_2-90% N_2 and 16 h at 600 °C under 10% O_2, 10% H_2O and N_2. Catalysts are noted Cu-FER@(X Na, P or Na + P), where X is the amount (μmol g^{-1}) of deposited inorganic compounds (Na, P or Na + P).

2.2. Structural/textural characterizations, elemental analysis

Elemental analyses were carried out to assess the copper, sodium and phosphorus loadings. After mineralization of the samples, analyses were performed with an ICP-OES apparatus (Perkin Elmer Optima 2000 DV). The effective Na, P or (Na + P) contents are reported in Table 1.

Specific surface areas were determined by the BET method using nitrogen adsorption at 77 K (Micromeritics ASAP 2000). Prior to the N_2 physisorption, the samples were degassed under vacuum 1 h at 90 °C and 4 h at 350 °C. The BET surface areas are listed in Table 1.

The powder XRD patterns were collected using an Empyrean (PANalytical) diffractometer. Data were recorded from 5° to 70° (2θ) with a scanning step of 0.017. Crystalline phases were identified by comparison with the ICDD database files.

2.3. Temperature programmed reduction (TPR) with hydrogen

Temperature programmed reduction experiments were performed on a Micromeritics Autochem 2920. Sample (100 mg) was placed in a U-shaped quartz reactor. Prior the reduction, the catalyst was *in-situ* calcined at 450 °C for 30 min under O_2 (heating rate: 5 °C min^{-1}). After cooling to room temperature and purge under argon flow for 45 min, the reduction was carried out under 1% H_2/Ar up to 1000 °C (rate: 10 °C

Table 1
Catalysts characterizations and NH_3-SCR activities at 250 °C and 500 °C in standard and fast-SCR.

	Sample	[X][a] (μmol g^{-1})	S_{BET} (m^2 g^{-1})	H_2-TPR (n_{H2}/n_{Cu})	NH_3-SCR (250 °C) (μmol g^{-1} min^{-1})		NH_3-SCR (500 °C) (μmol g^{-1} min^{-1})	
					Std-SCR	Fast-SCR	Std-SCR	Fast-SCR
	Cu/FER	0	352	1.02	67	309	93	298
Na	Cu/FER@(195 Na)	195	–	0.98	62	316	81	252
	Cu/FER@(235 Na)	235	–	1.00	61	307	57	183
	Cu/FER@(560 Na)	560	–	1.03	27	229	25	99
	Cu/FER@(830 Na)	830	270	1.04	15	171	13	42
P	Cu/FER@(170 P)	170	–	1.02	60	297	88	283
	Cu/FER@(290 P)	290	–	0.97	35	313	93	310
	Cu/FER@(480 P)	480	–	1.01	19	253	95	308
	Cu/FER@(560 P)	560	–	1.09	14	149	90	248
	Cu/FER@(750 P)	750	334	1.06	7	119	68	223
Na + P	Cu/FER@(215 Na + P)	215	–	1.01	52	267	94	289
	Cu/FER@(520 Na + P)	520	–	1.00	19	268	94	292
	Cu/FER@(735 Na + P)	735	308	1.00	11	198	85	254

[a] X = Na, or P, or Na + P inorganic compounds. 830 μmol_{Na} g^{-1} correspond to 1.9 wt-% Na; 750 μmol_P g^{-1} correspond to 2.25 wt-% P; 735 μmol_{Na+P} g^{-1} correspond to 0.84 wt-% Na and 0.84 wt-% P.

min^{-1}). The reduction was followed by a thermal conductivity detector (TCD). Because the TCD is sensitive to water, a H_2O trap was added downstream the reactor, allowing the quantification of the H_2 consumption. TPR profiles integration were performed to assess the H_2 consumption. The calculated H_2/Cu ratio is expected to be equal to 1 according to $Cu^{II} + H_2 \rightarrow Cu^{\circ} + 2\ H^{I}$ stoichiometry and based on the following assumptions: (i) copper species are all in + II oxidation state (Cu^{2+}, CuO, $CuAl_2O_4$) after the calcinations pre-treatment, (ii) Cu^{II} copper species are fully reduced into Cu° metallic copper at 1000 °C and (iii) no other species than Cu^{II} react during the TPR experiments.

2.4. Adsorption of nitric oxide and ammonia monitored by FT-IR

Information about the copper state in the various samples were obtained by NO adsorption monitored by infrared spectroscopy. In addition, adsorption of NH_3 was used to characterize ammonia adsorption behaviour. Note that the pyridine molecule usually employed to probe acid sites was not appropriate since it is not able to diffuse into the small porosity of the considered materials [18,19]. When ammonia is used, it interacts not only with the zeolite acid sites but also with the Cu^{2+} species, with possibly high Cu^{2+}/NH_x ratio as in $[Cu(NH_3)_5]^{2+}$ compounds observed by EPR in Cu-SSZ-13 [20]. Interestingly, the $[Cu(NH_3)_x]^{\delta+}$ complex formation appears reversible depending on the temperature and decompose around 250 °C in a large kind of zeolites [21]. As a consequence, the NH_3 adsorption measured at 250 °C was used to mainly describe the evolution of the Brønsted acid site amounts depending on the mineral contents.

IR spectra were collected using a Nexus Nicolet spectrometer equipped with a DTGS detector (deuterium triglyceride sulphur) and a KBr beam splitter. Spectra were normalized to a disc of 10 mg cm^{-2}. Before adsorption, the catalyst was *in situ* pre-treated under vacuum at 450 °C. Ammonia was adsorbed at 50 °C and desorption was performed up to 450 °C. NO adsorption was performed at room temperature, IR spectra were compared with the same n_{NO}/n_{Cu} ratio (around 30%) by adding a calibrated amount of NO in the infrared cell.

2.5. Catalytic activity

NH_3-SCR. The SCR tests were performed in a tubular quartz reactor. For the standard-SCR catalytic tests, 50 mg of zeolite (sieved in the 0.2 − 0.4 mm range) diluted in 50 mg of SiC (Prolabo, 0.35 mm) were used. The reactant gas composition was 500 ppm NO, 500 ppm NH_3, 10% O_2, 10% CO_2, 9% H_2O balanced in N_2. The total flow rate was fixed at 250 mL min^{-1}. For the fast-SCR catalytic tests, the inlet NOx mixture was composed of 250 ppm NO + 250 ppm NO_2, and only 15 mg of zeolite diluted in 15 mg of SiC were used in order to obtain conversions allowing the discrimination of catalysts. Gaseous NO, NO_2, NH_3, CO_2, O_2 and N_2 flows were adjusted by mass-flow controllers, while H_2O was added *via* a saturator. The composition of the feed gas and effluent stream were analysed online with a MKS 2030 Multigas infrared analyser. Catalytic tests were performed from 500 °C down to 150 °C by temperature steps of 50 °C. Catalytic activities were measured after stabilisation of effluent gases concentration.

NO and NH_3 oxidation activities. The NO and NH_3 oxidation tests were performed in similar condition than the standard-SCR tests. 50 mg of catalyst (sieved in the 0.2 − 0.4 mm range), diluted in 50 mg of SiC (Prolabo, 0.35 mm) were used. The gas compositions were 500 ppm NO or 500 ppm NH_3, 10% O_2, 10% CO_2, 9% H_2O balanced with N_2, with a total flow rate fixed at 250 mL min^{-1}. Gaseous effluent was monitored by a MKS 2030 Multigas infrared analyser. Oxidation activities were measured from 500 °C down to 100 °C. Due to the low catalytic activities in NO oxidation, results are presented at 450 °C, which undergoes a compromise between kinetic limitation and thermodynamic NO-NO_2 equilibrium. For NH_3 oxidation tests, ammonia conversion can reach 100% at 450 °C (essentially after Na addition). Therefore the results are presented for a temperature of 400 °C.

3. Results and discussion

3.1. Catalyst characterization

3.1.1. Structural/textural analysis

Fresh Cu-FER exhibited a specific surface area around 350 m^2 g^{-1} (Table 1). The addition of the mineral elements (Na, P) led to a decrease in the specific surface area, which is more pronounced in the case of sodium impregnation: it dropped to 270 m^2 g^{-1} and 334 m^2 g^{-1} after addition of 830 μmol_{Na} g^{-1} and 750 μmol_P g^{-1}, respectively. In both cases, the total pore volume appeared more affected than the microporous volume.

XRD patterns of the stabilized Cu-FER sample and the higher loaded catalysts in inorganic compounds are presented in Fig. 1. For all samples, XRD patterns are consistent with the ferrierite structure. Copper was not detected over the Cu-FER material, as already reported in [9,16]. After Na impregnation, the XRD pattern revealed the apparition of CuO, evidenced by the appearance of visible reflection at 2θ = 35.5° and 38.7° (insert in Fig. 1). To the opposite, no evolution of the diffraction peaks were evidenced for P and (Na + P)-containing catalysts. As a consequence, these first results suggest different impacts of inorganic compounds addition on the catalytic surface properties.

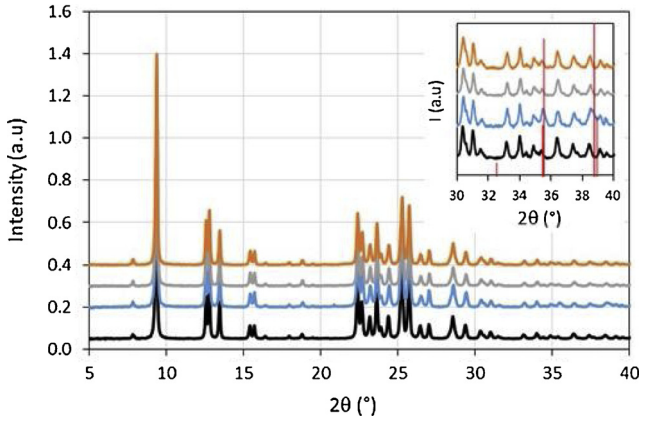

Fig. 1. XRD patterns of Cu/FER (–) and for the highest loaded samples in inorganic elements: (▬): Cu/FER@(830 Na), (▬): Cu/FER@(750 P), (▬): Cu/FER@(735 Na + P).

3.1.2. Copper characterization by temperature programmed reduction under hydrogen (H_2-TPR)

Usually, the reduction of exchanged copper-based zeolite results in two sequential reduction peaks. The first one is attributed to the reduction of exchanged Cu^{2+} species to Cu^{+} (300–350 °C depending of the host zeolite structure) and the second one at higher temperature (≈950 °C) corresponds to the final reduction of Cu^{+} to Cu° [8,16,22]. Instead, the reduction of external copper oxide outcomes by a one-step reduction of CuO species into metallic copper in the 200–400 °C temperature range [22,23]. Consequently, the first group of TPR peaks refers to the reduction of both Cu^{2+} and CuO species, into Cu^{+} and metallic copper, respectively.

Over zeolite-based samples, hydrothermal treatment may induce extra-framework aluminium (EFAL) formation, possibly leading thereafter to copper aluminate species ($CuAl_2O_4$) formation, which reduction peak is usually observed in the 450–550 °C temperature range [24].

H_2-TPR profiles corresponding to the catalysts with the higher Na, P or (Na + P) contents are reported in Fig. 2. Ferrierite host support reduction profile (not shown) did not exhibited any H_2 consumption. For all Cu-containing catalysts, the measured H_2/Cu ratio based on hydrogen consumption until 1000 °C was always very close to 1 (Table 1). It indicates a total Cu^{II} to Cu° reduction, whatever the added mineral(s). Consequently, there is neither evidence of copper stabilization in Cu^{I} state nor reduction of other species than Cu^{II}. In addition, the quantification of H_2 consumption depending on the H_2 reduction peak enables

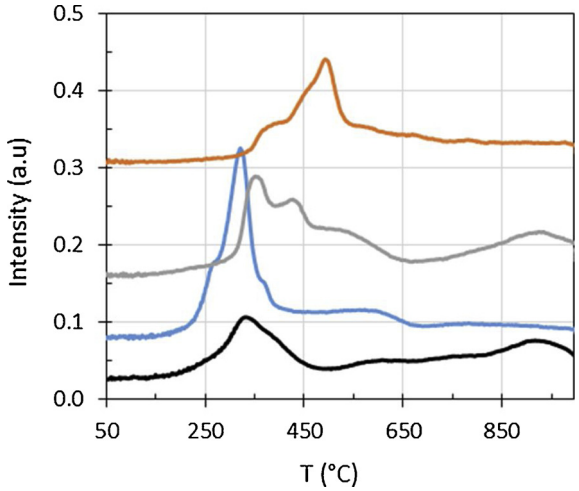

Fig. 2. Effect of the inorganic elements on H_2-TPR profiles of (–): Cu/FER, (▬): Cu/FER@(830 Na), (▬): Cu/FER@(750 P), (▬): Cu/FER@(735 Na + P).

the determination of the copper distribution in exchanged or external position.

The reduction profile of Cu-FER sample (without minerals addition) showed two main peaks, centred at 330 °C (including at shoulder at 390 °C) and 950 °C, associated to the two steps reduction process of exchanged Cu^{2+} species *via* the intermediate formation of Cu^{+} species. Note that several isolated Cu^{2+} species were expected in exchanged position depending on the amount of nearby framework negative charges. The consensus is that two main Cu active sites are possible, namely Cu^{2+} or $[Cu(OH)]^{+}$ species. In fact, Cu^{2+} ions located at different cationic sites have different binding energies with the framework. The Cu species with one Al bond ($[Cu(OH)]^{+}$-Z) appear reducible at lower temperature than Cu^{2+} units (Cu^{2+}-2Z) [25]. As a consequence, the reduction peak observed at 330 °C and 390 °C may correspond to the reduction of the two types of Cu^{2+} species into Cu^{+}. In addition, a broad reduction peak in the 500 °C – 800 °C temperature range was also denoted, assigned to $CuAl_2O_4$ reduction. Based on the amount of H_2 consumed for reduction peak at 950 °C, it was estimated that 92% of copper was in exchange position before Na and/or P deposits.

The addition of 830 μmol g^{-1} Na (blue curve, Cu-FER@(830 Na) led to a shift of the first reduction peak to the lower temperature and to the disappearance of the higher temperature reduction peak at 950 °C related to the second step of copper reduction in exchanged position. The decrease in the temperature of copper reduction with the increase in the sodium content as cocation was also evidenced in [22,26]. For the Cu-FER@(830 Na) sample, the loss of copper in exchanged location was balanced by an increase in the overall area of the first reduction peak, reflecting the formation of external copper oxide, in accordance with the XRD analysis (Fig. 1). Indeed, 76% of copper in Cu-FER@(830 Na) were then CuO type species.

Concerning P-containing catalysts, different results were denoted compared to the Na-samples. A representative TPR profile, recorded with Cu-FER@(750 P), is presented Fig. 2 (grey curve). A shift to higher temperature of the low temperature reduction peaks was observed, while the consumption of hydrogen at high temperature (950 °C) appeared just a little affected. This profile points out a direct interaction between exchanged copper and phosphorus, which led to a delay in the onset reduction of exchanged copper. Note that similar shift to higher temperature was also observed for CuO species deposited on silica after phosphorus addition [27]. More precisely, Sepúlveda et al. observed a decrease in the CuO reduction peak with the appearance of a new peak at higher temperatures assigned to copper phosphate or copper in interaction with phosphorus. Similar results were also reported by Mamontov et al. [28]. To obtain further information about the Cu-P interaction, IR analysis of skeleton vibration bands were performed over P-containing catalysts and fresh Cu-FER sample (for these measurements, 1.15% of catalyst was diluted in KBr as self-supported wafer). The Cu—O stretching vibrations in the wavenumber range between 500 and 650 cm^{-1} was particularly studied [29,30]. It appears that phosphorus free sample exhibits a band centered at 589 cm^{-1} assigned to Cu—O stretching vibration while a shift to 590 cm^{-1} was observed for Cu-FER@(750 P) sample (results not shown). This shift is consistent with a Cu—P interaction since phosphorus atom is lighter than copper atom: the substitution should result in an upward shift of the vibration wavelength according to the well-established theories of vibrational modes.

Interestingly, the TPR profile obtained after the co-addition of Na + P (orange curve, Cu-FER@(735 Na + P)) shows intermediate behaviors, with both a decrease in the exchanged copper content (sodium contribution, favouring the CuO formation) and a shift of the onset reduction of copper species to higher temperature (phosphorus contribution).

As previously mentioned, H_2-TPR profiles were deconvoluted to assess the effect of inorganic compounds toward the copper distribution. The H_2 consumption related to the peak centred at around 950 °C

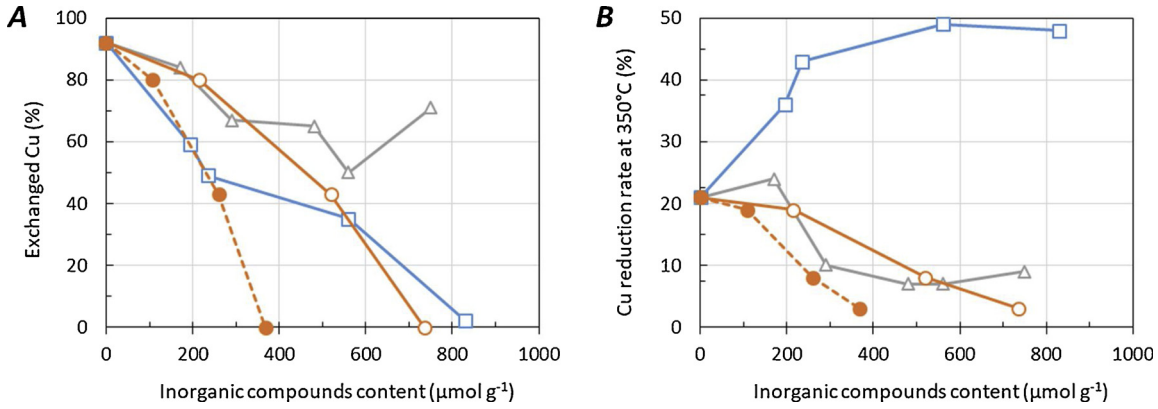

Fig. 3. Exchanged copper distribution (A) and copper reduction rate up to 350 °C (B) in function of inorganic compounds content. (□, ▬, ▬): Cu/FER@(Na), (△, ▬, ▬): Cu/FER@(P), (○, ▬, ▬): Cu/FER@(Na + P); dotted lines (●, ---) correspond to data plotted depending on only Na or P contents ([Na] = [P]).

(attributed to Cu^+ reduction located in exchanged position) was calculated to evaluate the amount of copper in exchanged position in function of the inorganic compounds content (Fig. 3-A).

As already reported in [16], the decrease in copper species in exchanged position, associated with the CuO formation, is linearly correlated with the Na content (Fig. 3-A, blue curve). This is attributed to a switch between Na^+ and Cu^{2+} species in exchanged position in the zeolite skeleton. The exchanged copper ratio was also affected by phosphorus addition (Fig. 3-A, grey curve), but in lower extent compared with the sodium impact. About 65–70 % of the copper was maintained in the exchange position for the highest phosphorus content. Again, this result illustrates diverse behaviours of inorganic compounds toward the Cu-FER catalyst.

With the simultaneous equimolar addition of Na and P (Fig. 3-A, orange curve), the exchanged copper content decreased first following the behavior already observed when adding only P. However, the effect of (Na + P) can be also considered depending on each Na or P molar content, which are equal since phosphorus and sodium were co-impregnated from H_2NaPO_4 salt (Na content = P content = half of the total inorganic compounds molar content). With this point of view (Fig. 3A, dotted orange line), it appears that the simultaneous addition of (Na + P) rather leads to a behavior close to single Na-containing materials. For the highest (Na + P) content (750 µmol.g^{-1}), exchanged copper was not detected in the zeolite.

In order to take into account the observed shift in the TPR profiles with the phosphorus additions, the H_2 consumption in the 20–350 °C temperature range was also calculated and reported Fig. 3-B depending on the inorganic compounds content. The temperature of 350 °C was chosen because it corresponds to the maximum of H_2 consumption of the first reduction peak of minerals-free catalysts (Fig. 2). Note that this parameter is not suitable for catalysts containing only sodium since Na addition induced the formation of CuO species which were reduced by H_2 below 350 °C. Consequently, an increase in the H_2 consumption in the 20 °C–350 °C temperature range was then observed (Fig. 3-B, blue curve). With the increase of phosphorus concentration (Δ), the amount of Cu compounds reduced at 350 °C decreased, and stabilized at around 10% from approximately 300 $\mu mol_P\, g^{-1}$. This illustrates strengthened Cu-P interactions with the addition of phosphorus. Same behaviour was also noticed after (Na + P) co-poisoning. However, for same amount of P deposited, the H_2 consumption measured until 350 °C was lower than in presence of Na (gray curve compared to orange dotted curve). It highlights the fact that P interacted also with the copper species generated by Na addition.

The chemical alterations of the catalyst surface by minerals co-addition are discussed furthermore in the Section 3.4.1, where the reducibility at 350 °C is used to account of the modifications induced by the presence of phosphorus on the NO and NH_3 catalytic performance of materials. To summarize, the characterization of the copper state by H_2-TPR after the (Na + P) co-addition showed that both elements affected the catalyst, with simultaneously a Cu^{2+}-Na^+ back-exchange (leading to CuO formation) and copper-phosphorus interactions (which induce the reduction of copper species at higher temperature).

3.1.3. Acidic sites characterization: IR spectra of free OH groups

The stretching OH region of FTIR spectra provides information on the acidity of the zeolite and its evolution as a function of the added minerals. Fig. 4 compares the spectrum related to Cu-FER sample with those recorded with samples containing the highest minerals contents. Cu-FER sample exhibited four OH bands after activation at 450 °C. The band at 3747 cm^{-1} is assigned to single terminal Si—OH groups. The component at 3724 cm^{-1} is characteristic of O—H stretching of geminal silanols and/or weakly perturbed vicinal pairs of terminal silanols [18]. One tailed band for bridged Al—(OH) —Si hydroxyls at 3602 cm^{-1} was also denoted. This is characteristic of the Ferrerite zeolite Brønsted acid sites, associated with the 8 and 10-membered ring channels. The band at 3642 cm^{-1} is assigned to Al—OH extra-framework groups due to EFAL species induced by thermal treatment.

The impregnation of Na led to a decrease of about 80% in the intensity of the OH band at 3602 cm^{-1}, assigned to Brønsted acid sites. It

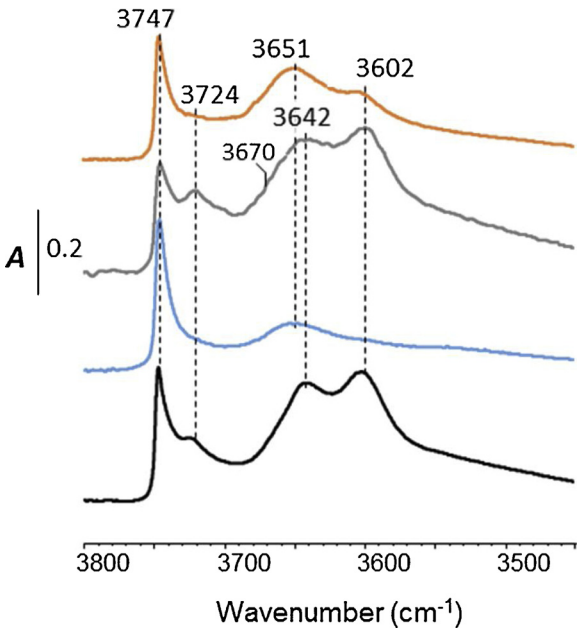

Fig. 4. IR spectra in the $\nu_{(OH)}$ region of (–) Cu/FER sample and materials with the higher content in minerals-contain: (▬) Cu/FER@(830 Na); (▬): Cu/FER@(750 P); (▬): Cu/FER@(735 Na + P).

is assumed that a large part of the H^+ ions in the zeolite framework was exchanged by Na^+ ions during the impregnation. In addition, the initial band of EFAL species at 3642 cm^{-1} was also affected, with both a decrease of its intensity (-60%) and a shift to the higher wavenumber at 3651 cm^{-1}. On the contrary, no significant change was observed in the OH stretching region of Cu-FER@(750 P), with the exception of a slight shoulder at 3670 cm^{-1}. Note that stretching vibration of terminal P—OH groups are observed around 3672 – 3666 cm^{-1} over $AlPO_4$ and SAPO materials [31]. It induces that Brønsted acidity could be slightly modified over the P-containing sample. Nevertheless, the acidity of the studied zeolite appeared relatively unaffected by the addition of phosphorus compared to the sodium impregnation. With the co-addition of (Na + P), a decrease in the intensity of both EFAL (3642 cm^{-1}) and bridged (3602 cm^{-1}) hydroxyl groups was observed. It appears that Brønsted acid sites were partly poisoned by the simultaneous addition of (Na + P), as markedly noticed for Na deposition only. Finally, only sodium affected the Brønsted acid sites, either added alone or combined with P.

The characterization of acidic sites was supplemented by adsorption of basic probe molecule (NH_3) monitored by FTIR.

3.2. NO and NH_3 activation

3.2.1. NO and NH_3 adsorption monitored by FTIR

NO molecule was used to investigate the oxidation state of copper cations in zeolites, due to its ability to form stable nitrosyl adducts with copper ions. IR spectra of adsorbed NO are reported in Fig. 5-A. Spectrum corresponding to mineral free Cu-FER was characterized by a band at 1909 cm^{-1} assigned to nitrosyl [Cu^{2+}–NO] complex having a square pyramidal configuration. After Na addition, the band at 1909 cm^{-1} was shifted to lower wavenumbers, at 1897 cm^{-1}. As previously commented in [16], the component at 1897 cm^{-1} is attributed to Cu^{2+} sites with a square planar configuration and adjacent to a single framework aluminum atom. It highlights a modification of the copper site location after Na addition. After P deposits, no wavenumber modifications were denoted. It indicates that location of Cu^{2+} exchanged species were then not affected. However, the $\nu_{(NO)}$ area was strongly altered. These results indicate Cu-P interactions that partially inhibited the accessibility of exchanged copper species. Similar tendencies were denoted after (Na + P) addition. Note that a shoulder was observed at 1897 cm^{-1}, corresponding to nitrosyl compounds previously observed over Cu/FER@(830 Na). Obviously, Na or P have different effects over Cu species, as already pointed out by other described characterization techniques.

Ammonia adsorption was also monitored by FT-IR. The spectral region of N—H stretching vibrations (3500 – 3000 cm^{-1}) is relatively complex, because the distortion of the NH_3 molecule upon coordination leads to a splitting of the $\nu_{N–H,asym}$ mode and to the activation of the $\nu_{N–H,sym}$ mode. Consequently, IR analysis were performed in the N—H bending modes of adsorbed ammonia, as illustrated in Fig. 5-B. After evacuation at 50 °C, Cu-FER sample was dominated by absorption bands at 1452 and 1397 cm^{-1} (δ_{asym}), which are usually assigned to ammonium ions formed by the protonation of ammonia molecules located on Brønsted acid sites. These two components are tentatively assigned to different types of hydrogen-bonded ammonium, including monodentate and bidentate complexes for instance. The sharp band at 1621 cm^{-1} is assigned to bending modes of ammonia coordinatively bound to Lewis acid sites (δ_{asym}). The nature of these sites could be either tricoordinated Al atoms or Al species attached to defective sites, related to framework and extra-framework positions, or also copper Lewis sites responsible of $[Cu^{I}(NH_3)_2]^+$ or $[Cu^{II}(NH_3)_4]^{2+}$ complexes formation [32]. The addition of 830 µmol g^{-1} of Na led to the total disappearance of the δ_{asym} bands at 1452 and 1397 cm^{-1} assigned to ammonia protonated on Brønsted acid sites. These results are consistent with the IR spectra in $\nu_{(OH)}$ region which showed the loss of bridged zeolitic hydroxyls after addition of a high sodium level. Over Cu-FER@(750 P) catalyst, IR spectrum was substantially unchanged, with only a slight decrease in the intensity of the $\delta_{(NH)}$ band at 1621 cm^{-1} assigned to ammonia coordinated on Lewis acid sites. Again, this result is in agreement with the study of free hydroxyl groups. As expected, the simultaneous addition of (Na + P) led to intermediate results and the impact of both elements were detected. Note that the bands at 1452 and 1397 cm^{-1} were still observed after (Na + P) addition, which indicates that the Brønsted acidity remained partially maintained, as for the samples modified by phosphorus, but unlike those containing sodium.

In addition, the bands at 1452 – 1397 cm^{-1} and 1621 cm^{-1} were used to quantify the amounts of Brønsted and Lewis acid sites, respectively. The molar extinction coefficient values ($\varepsilon_{Brønsted}$ = 4.6 cm µmol^{-1}, ε_{Lewis} = 1.1 cm µmol^{-1}) were both determined at the laboratory by successive addition of controlled amount of NH_3 [16]. Fig. 6 depicts the evolution of total ammonia adsorption capacity (on Brønsted and Lewis acid sites, but also on copper species) in function of both the temperature desorption and the loading in Na, P or (Na + P). The ammonia adsorption capacity of the mineral-free Cu-FER sample (■) decreased with the temperature, from 2150 µmol g^{-1} to 335 µmol g^{-1} in the 50–250 °C temperature range. After minerals addition, NH_3 adsorption capacities were always lower than in Cu-FER reference catalyst. For instance, ammonia adsorption was around 990 µmol g^{-1} at 50 °C and 5 µmol g^{-1} at 250 °C for Cu-FER@(830 Na) sample (■).

To point out the influence of Na and/or P contents on the ammonia

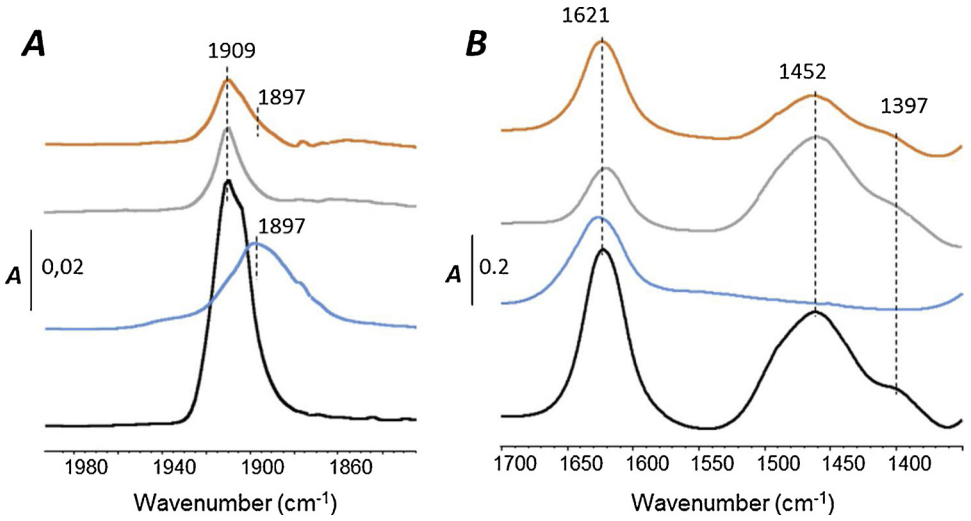

Fig. 5. IR spectra of Cu/FER sample and materials with the highest mineral loading. (A): $\nu_{(NO)}$ region after NO adsorption at RT; (B): $\delta_{(NH)}$ region after NH_3 adsorption and evacuation at 50 °C. (–): Cu/FER, (▬): Cu/FER@(830 Na), (▬): Cu/FER@(750 P), (▬): Cu/FER@(735 Na + P).

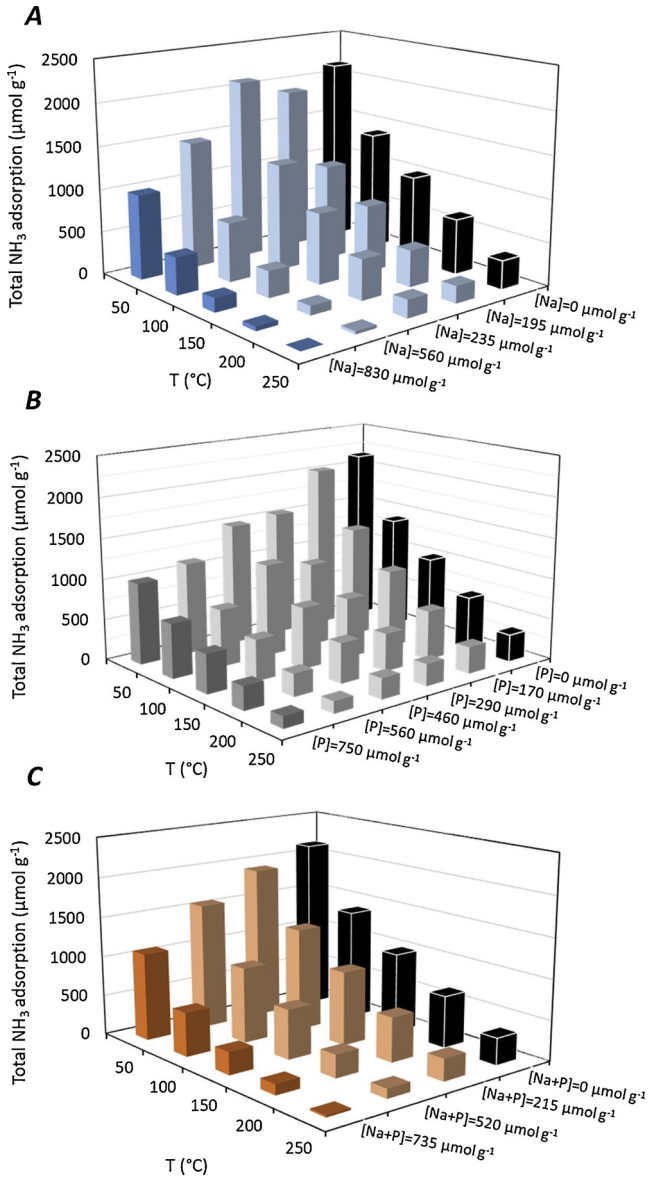

Fig. 6. Ammonia adsorption capacities in function of temperature and inorganic compounds content for (A): Na addition; (B): P addition; (C): Na + P addition. (■): Cu/FER, (■): Cu/FER@(830 Na), (■): Cu/FER@(750 P), (■): Cu/FER@(735 Na + P). Data tags represent the amount of minerals (Na, P or Na + P) added in µmol g^{-1}.

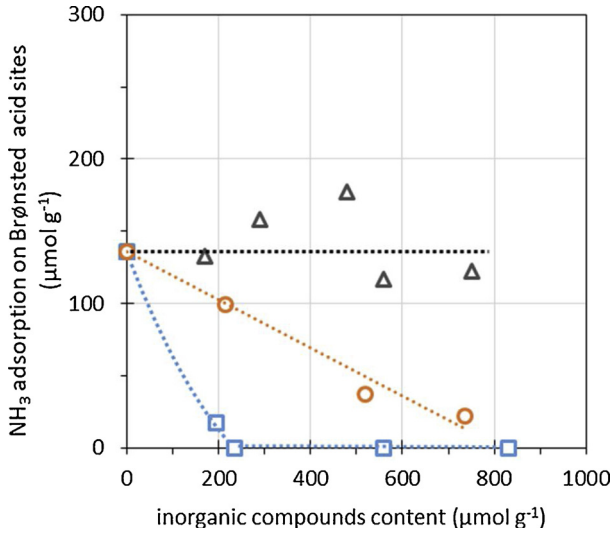

Fig. 8. Ammonia adsorption capacities at 250 °C from IR bands centered at 1452 and 1397 cm^{-1}, assumed to correspond only to the Brønsted acid sites of the zeolite. Influence of the mineral loading. (□, —, —): Cu/FER@(Na), (Δ, —, —): Cu/FER@(P), (○, —,—): Cu/FER@(Na + P).

adsorption capacities, data from measurements at 50 °C and 250 °C are reported in Fig. 7-A and -B, respectively. At 50 °C, tendencies were very close for all types of poisoning. One mole of added mineral appeared to poison 1.5 mol of NH_3 adsorption site. Different behaviors were observed at higher temperatures. Compare to Na poisoning, the ammonia adsorption capacities were less affected by phosphorus addition. Some ammonia was still adsorbed at 250 °C even on the most phosphorus-loaded material (Fig. 7-B). It induces that the impregnation of phosphorus selectively poisoned weaker acid sites. Indeed, the strongest acid sites, assigned to bridged OH groups, remained less sensitive to the phosphorus addition compared to the opposite of Na poisoned samples (Fig. 4).

After the simultaneous addition of both Na and P, the NH_3 adsorption capacities were rather close to those recorded with Na-containing materials, with zero NH_3 adsorption for the highest (Na + P) level (Cu-FER@(735 Na + P), ■) at 250 °C.

To highlight especially the evolution of the Brønsted acid sites depending on the mineral contents, measurements at 250 °C appear suitable because the $[Cu(NH_3)_4(H_2O)_x]^{2+}$ complexes (with $x = 1, 2$) are then supposed to be decomposed [21]. Fig. 8 reports the influence of the mineral loadings on the NH_3 adsorption at 250 °C from the integration of the IR bands centered at bands at 1452 and 1397 cm^{-1} assigned to the Brønsted acid sites. This figure clearly confirms that the

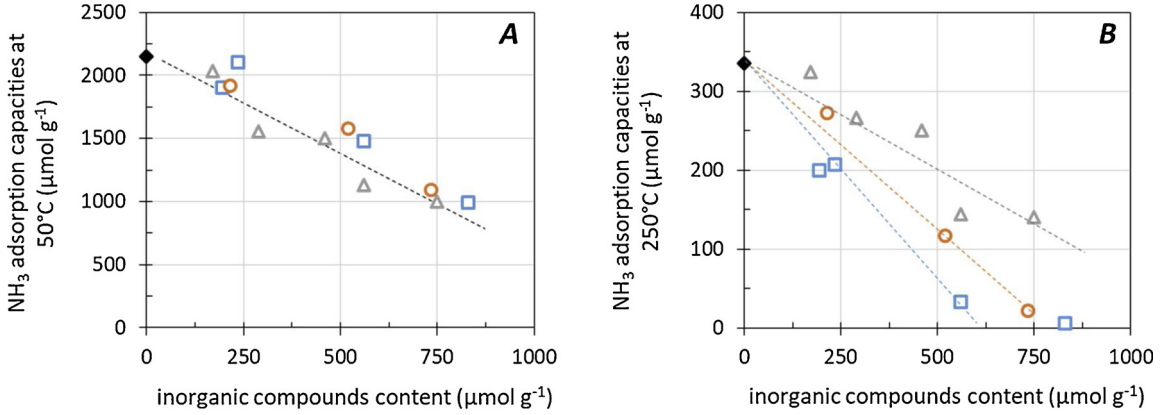

Fig. 7. Effect of minerals addition on NH_3 adsorption capacities at (A): 50 °C and (B): 250 °C (◆: Cu/FER; □, —: Cu/FER@(Na); Δ, —: Cu/FER@(P); ○, —: Cu/FER@(Na + P)).

sodium addition strongly affected the Brønsted acid sites of the zeolite, even at low loading. No more Brønsted acid sites were available for ammonia adsorption at 250 °C for the Cu-FER@(235 Na) sample. On the contrary, the Brønsted acid sites probed at 250 °C were not affected by phosphorus additions, while the total amount of adsorbed NH_3 decreased, especially at low temperature (Fig. 7). Then, this overall decrease was only attributable to a limitation of ammonia adsorption on copper species, due to the Cu^{2+}-P interaction.

With the Cu-FER@(Na + P) samples, an intermediate behavior was obtained. In fact, a linear decrease was recorded in Fig. 8 depending on the (Na + P) loading. It is then only attributable to the sodium behavior which poisoned the Brønsted acid sites. Measurements at 250 °C clearly indicated that Na was the major responsible for the decrease in the NH_3 adsorption attributed to Brønsted acid sites poisoning. This observation is in accordance with results previously reported in Fig. 4 related to the $\nu_{(OH)}$ region of the FTIR spectra.

Finally, these results highlight different impacts of Na and P towards surface chemistry of catalysts. The diminution of NH_3 adsorption capacities of Na-containing sample is assigned to both a poisoning of the zeolite acid sites and a loss of Cu^{2+} adsorption sites caused by a Cu^{2+}-Na^+ back exchange (together with a migration the Cu species to form CuO). Phosphorus acts differently, Cu-P interactions are advanced to explain the NH_3 adsorption capacities diminution while the Brønsted acidity appeared unaffected. Impacts of both elements were evidenced after (Na + P) co-addition.

3.2.2. NO and NH_3 oxidation behaviors

The effect of inorganic compounds (Na, P and Na + P) toward NO and NH_3 oxidation activities were evaluated in the 100 °C–500 °C temperature range.

The oxidation of NO to NO_2 is reported as the limiting step for the standard-SCR reaction, involved to reach the most favourable fast-SCR stoichiometry [7]. The mechanism of the NO oxidation are still in debate. For instance, Janssens et al. [6] proposed that NO oxidation occurs *via* an activation catalytic cycle involving NH_3 over Cu zeolite, rather than a single reaction step. However, the SCR activity is clearly enhanced at low temperature since NO and NO_2 are feed together because it favours the formation of N^{-III} species (like HONO, obtained by the following reaction: $NO + NO_2 + H_2O \rightarrow 2\ HONO$) which are able to react with N^{+III} species (like NH_3) to form N° species. In fact, the NO activation corresponds to its partial oxidation. It could occurs *via* the participation of NO_2 but in absence of NO_2, the reaction rate at low temperature appears limited by O_2 activation [33,34]. Anyway, NO oxidation tests are suitable to highlight the evolution of the redox function of the Cu-FER catalyst with Na and/or P additions. Since NO oxidation experiments revealed low activities, only results recorded at 450 °C are reported in Fig. 9. At this temperature, the NO_2 storage should be negligible [35]. Note that a further increase in the temperature does not allow to discriminate the materials due to the thermodynamic NO-NO_2 equilibrium.

The ammonia oxidation by oxygen is not desired since it induces an overconsumption of the reductant with regard to the NH_3-SCR process. However, it also accounts for ammonia activation for the whole catalysts. Activities reported in Fig. 9-B were measured at 400 °C. For higher temperatures, ammonia conversion could reached 100%, especially for Na-containing samples. Note that whatever the temperature, no N_2O was detected during ammonia oxidation experiments.

The addition of sodium (□) initially led to the increase in NO and NH_3 oxidation activities until Na contents close to 200 $\mu mol_{Na}\, g^{-1}$. For the Na contents higher than 560 $\mu mol_{Na}\, g^{-1}$, NO and NH_3 oxidation activities decreased. Note that the ammonia oxidation was fully selective into N_2 over Cu-FER, except with the higher Na loaded sample for which the formation of NOx (mainly as NO, with traces of NO_2) was also observed despite the overall decrease in the ammonia oxidation activity. The maximum NOx ($NO + NO_2$) selectivity was measured at 500 °C and reached 35% for the Cu-FER@(830 Na) sample (results not shown). Note that the emission of NOx compounds related to NH_3 oxidation was only observed over sodium-poisoned catalysts, *i.e.* with materials exhibiting CuO species.

Phosphorus additions (Δ) led to a continuous decline in NO and NH_3 oxidation activities, substantially steeper than for sodium poisoning. The oxidation rate of NO, initially from 8% (0.0078 mmol $g^{-1}\, h^{-1}$), dropped to 2% (0.0016 mmol $g^{-1}\, h^{-1}$) after addition of 750 $\mu mol\, g^{-1}$ of phosphorus, corresponding to a loss of 75% of the initial activity. For the NH_3 oxidation activity, similar tendencies were observed, with a drop of 86% of the initial activity after addition of 750 $\mu mol_P\, g^{-1}$. This result clearly highlights the inhibitor effect of the phosphorus addition on the redox behavior of Cu^{2+} copper species.

For the simultaneous addition of phosphorus and sodium, the results are presented either depending on the total deposited poison contents (solid line, symbols ○), or depending on-the amount of each Na or P element (which were equal, dotted line, symbols ●). Fig. 9 shows that the deactivation due to the co-addition of sodium and phosphorus (○,●) appeared mainly related to that of phosphorus alone (Δ), especially for the higher contents. However, the recalculated curve corresponding to Na or P contents in the (Na + P) co-addition shows a more negative effect than the combination of each components alone. It means that in presence of Na, phosphorus interacts not only with exchanged Cu^{2+} units (from results obtained with Cu-FER@(P) samples) but also with CuO species (resulting from Na^+/Cu^{2+} back exchange). CuO species appeared responsible for the enhancement of the oxidation behaviour after single Na addition, but CuO appeared also inhibited

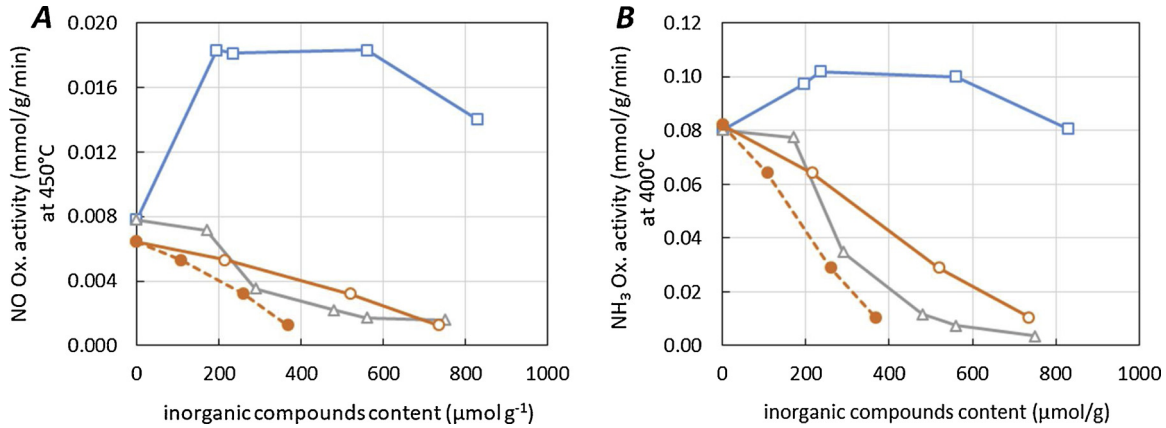

Fig. 9. A: activity in NO oxidation at 450 °C (maximum recorded activity corresponded to 18% NO conversion) and (B): activity in NH_3 oxidation at 400 °C (maximum recorded activity corresponded to 100% NH_3 conversion) in function of inorganic compounds content. (□, ▬, ▬): Cu/FER@(Na), (Δ, ▬, ▬): Cu/FER@(P), (○, ▬, ▬): Cu/FER@(Na + P); dotted lines (●, ---) correspond to data plotted depending on only Na or P contents ([Na] = [P]).

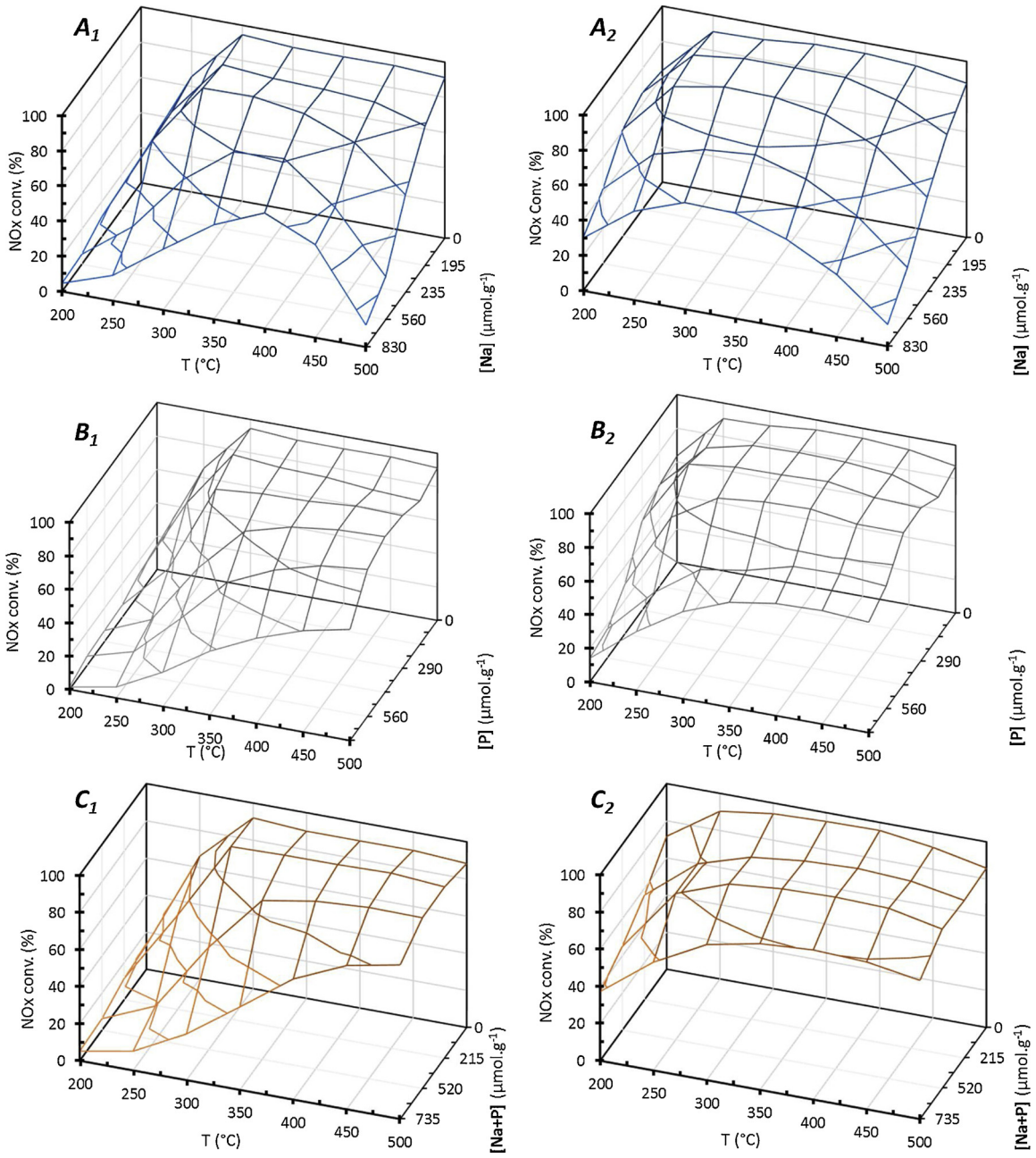

Fig. 10. NH_3-SCR performances in standard (1) and fast (2) condition in function of temperature and inorganic compounds content for (A): Na addition; (B): P addition; (C): Na + P addition. (▬): Cu/FER@(Na), (▬): Cu/FER@(P), (▬): Cu/FER@(Na + P).

when phosphorus was co-added (Cu-FER@(Na + P) samples). This specific point is discussed subsequently in the Section 3.4.1.

3.3. NH_3-SCR performances

Catalytic performances of all the studied catalysts were evaluated in both standard and fast NH_3-SCR conditions. NOx conversions are presented in Fig. 10 depending on both the temperature test and the mineral loading. Remind that the catalytic tests in fast-SCR condition were performed with lower amount of catalyst (15 mg *versus* 50 mg for the standard-SCR condition) to limit the DeNOx efficiency and possibly distinguish a deactivation by inorganic compounds addition.

In standard-SCR condition, the reference Cu-FER catalyst exhibited a limited NOx conversion for temperature lower than 300 °C (14% and 66% at 200 and 250 °C, respectively). Beyond 300 °C, the NOx conversion reached 91–95%. In fast-SCR condition, the conversion was obviously increased despite the lower amount of implemented catalyst, with 63% of converted NOx at 200 °C. Ammonia conversions (not shown) for both standard and fast-SCR were similar than NOx ones. The competitive reaction with ammonia oxidation was only observed in fast SCR condition for temperatures higher than 450 °C. Moreover, N_2O emissions were very limited. The maximum N_2O outlet concentration was 4 ppm, recorded at 500 °C in fast-SCR condition.

Na additions clearly led to a drop in the DeNOx efficiency in standard-SCR condition (Fig. 10-A_1), especially for sodium contents higher than 235 µmol g^{-1}. The catalytic deactivation was observable in the whole temperature range. For instance, 50% of the initial activity was lost at 250 °C after approximately 450 µmol g^{-1} of Na deposit together with a strong deactivation at higher temperature resulting in a relative loss of 86% at 500 °C for Cu-FER@(830 Na). A competition between the NOx reduction reaction and the ammonia oxidation reaction, leading to a lack in ammonia to reduce NOx, is advanced to explain the NOx

conversion drop at high temperature. This explanation is supported by a full ammonia conversion at high temperature over Cu-FER@(830 Na) (results not shown), together with the NH_3 oxidation behaviours previously commented in Fig. 9-B. In fast-SCR condition (Fig. 10-A_2), similar evolutions of the NOx conversions were denoted.

Over Cu-FER@(P) catalysts, until 170 $\mu mol_P\ g^{-1}$, the NOx conversion in standard-SCR condition remained unaffected up to 300 °C (Fig. 10-B_1). For higher phosphorus contents, the NOx conversion was significantly decreased, reaching only 6% at 250 °C for the Cu-FER@(750 P) sample. Consequently stronger deactivation was achieved with phosphorus addition compared to Na-containing samples. Obviously, phosphorus appeared the most penalizing mineral to the DeNOx efficiency at low temperature. Results are partially consistent with the evolutions in NO oxidation behavior reported in Fig. 9-A. interestingly, compared with sodium catalysts, the DeNOx activity was relatively maintained at high temperature. For instance, the NOx conversion at 500 °C reached 66% on Cu-FER@(750 P), compared with 12% for Cu-FER@(830 Na) material. In addition, the ammonia conversion over the P-containing catalysts remained similar to that of NOx (results not shown). Consequently, the ammonia oxidation did not compete with NOx reduction, unlike sodium-poisoned samples. It suggests a poisoning of the redox properties of copper by phosphorus, without altering the Cu location (CuO formation for instance), as previously advanced by means of NO adsorption monitored by FTIR for instance (Fig. 5-A). As for the Na-poisoned catalysts, fast and standard-SCR conditions (Fig. 10-B_2) led to same tendencies.

Catalysts poisoned by the simultaneous addition of Na and P (Fig. 10-C) exhibited deactivation trend closer to that observed on the P-catalysts. The decrease in NOx conversion was especially significant in the low temperature domain, while the DeNOx efficiency at high temperatures appeared less effected.

The next section attempts first to represent the influence of each studied mineral on the catalyst surface functions and secondly to correlate these behaviors with the catalytic activities.

3.4. General trends in catalyst deactivation

3.4.1. Poisoning of chemical functions by inorganic compounds deposits

Based on the characterization technics used, this part aims to highlight the impacts of sodium and/or phosphorus on the Cu-FER sample surface properties. H_2-TPR experiments enabled to assess to the evolution of the copper species distribution (exchanged species, external CuO), especially depending on the sodium additions. Moreover, changes in copper species reducibility with phosphorus additions indicated interactions with the added mineral. These results were in accordance with the NO adsorption experiments monitored by FTIR. NH_3 adsorption experiments monitored by FTIR gave information about both the copper availability and the Brønsted acidity. Both are consistent with results deduced from the H_2-TPR experiments and the FTIR spectra of the OH region, respectively. Supplementary information were obtained by examination of the redox behavior from NO and NH_3 catalytic tests since the various copper species exhibit various oxidation behavior.

The relationships between copper species evolution (expressed as either the exchanged Cu^{2+} ratio or the copper reduction rate at 350 °C, both from TPR profiles) and the catalytic oxidation behaviors (NO and NH_3 oxidation) are described Fig. 11 depending on the Na and/or P addition. Fig. 11-A shows that both NO and NH_3 oxidation reactions cannot be directly associated with the exchanged Cu^{2+} ratio, despite the redox function was expected to be sensitive to the copper distribution. Indeed, different trends were observed depending on Na and/or P addition. Samples containing phosphorus showed a decrease in the oxidation behaviors while Cu-FER@(Na) samples exhibited a maximum. In fact, the oxidation reactions appeared rather related with the copper reducibility at low temperature, especially for P-containing catalysts (Fig. 11-B). Based on all the collected data, the interactions of each added mineral with the Cu-FER active sites are summarised and illustrated below.

3.4.1.1. Na-containing samples.. After Na deposits, NH_3 adsorption capacities decreased (Fig. 7). It is attributable to both (i) a loss of Brønsted acid sites, evidenced in Fig. 8 and also in the $\nu_{(OH)}$ stretching region of IR spectra (Fig. 4) and (ii) a loss of exchanged Cu^{2+} species since a back-exchange of Cu^{2+} with Na^+ occurred, associated with the formation of external Cu species, detected as CuO (H_2-TPR and XRD analyses). This CuO species are reported as active species for both NO and NH_3 oxidations. Consequently, Cu-FER@(Na) catalysts exhibited an improvement in the oxidation behaviors (Fig. 11-A). The volcano shape curve in Fig. 11-A can be attributed to a CuO sintering for the highest Na loadings, in which no more copper appeared located in exchange positions. Note that, the apparent improvement in the oxidation behaviors reported in Fig. 11-B was also related to the formation of external CuO, because it induced therefore a higher reduction rate at low temperature during the H_2-TPR experiments (Section 3.1.2). A schematic illustration of the active sites poisoning by sodium is proposed in Scheme 1.

3.4.1.2. P-containing samples.. After P addition, the exchanged Cu^{2+} species remained moderately affected: for the higher minerals loadings, the relative higher loss was approximately 30% compared to 100% for Na-containing sample (Fig. 3-A). In fact, the apparent decrease in the oxidation behaviors observed with the decrease of the exchanged Cu^{2+} ratio (Fig. 11-A, gray curve) is not the driving force since Na-containing samples exhibited another trend (blue curve). The main influence of phosphorus was made of direct interactions with copper, as illustrated by the reduction profiles (Fig. 2). These interactions were primarily responsible for catalyst deactivation toward the oxidation reactions (Fig. 11-B). NH_3 adsorption capacities were also altered (Fig. 6). However, unlike sodium deposition, the Brønsted acid sites were obviously not poisoned by phosphorus (Figs. 4 and 8). In accordance with this result, the relative loss in NH_3 adsorption at 250 °C for P-containing samples was lower than over Na-containing samples. The drop in ammonia adsorption capacity was then attributed to the blocking of the Cu^{2+} adsorption sites by phosphorus. Taking into account the overall observations, the phosphorus poisoning effect over the catalyst surface is summarized in Scheme 2. The exact nature of the phosphate oxyanion that balances the charge of the exchanged Cu^{2+} units remains unknown and the possible formation of metaphosphate (PO_3^-), hydrogen phosphate (HPO_4^{2-}) and dihydrogen phosphate ($H_2PO_4^-$) can be envisaged.

3.4.1.3. (Na + P)-containing samples.. After the simultaneous equimolar addition of phosphorus and sodium, a combination of deactivation mechanisms underwent by Na or P deposits alone. Both exchanged copper ratio and Cu species reducibility were affected by (Na + P) addition (Fig. 3). In fact, a beneficial effect provided by Na could be expected in the NO and NH_3 oxidation tests, due to the formation of CuO species. However, lower oxidation activities were recorded after (Na + P) addition (Fig. 9), indicating that the new formed Cu-species also interacted with phosphorus. Otherwise, bridged OH groups were partially inhibited by the (Na + P) deposits. In fact, this was attributable to the Brønsted acid sites substitution by Na^+ species (Fig. 8). Due to limited amount of Na in the higher (Na + P) studied catalysts, some Brønsted acid sites were maintained (Figs. 4 and 8). Nevertheless, phosphorus also contributed to the decrease in the ammonia adsorption behavior because phosphorus inhibited the NH_3 adsorption on copper species. Note that we have recently showed that CuO species were less affected by phosphorus addition compared to exchanged Cu^{2+} species [36]. Definitely, sodium compete with both the acidic hydroxyl groups and the copper unit in exchanged position. Interestingly, Fig. 3 (dotted orange line *vs*. blue line) evidenced that for sodium content higher than 250 $\mu mol\ g^{-1}$, the loss of exchanged Cu^{2+}

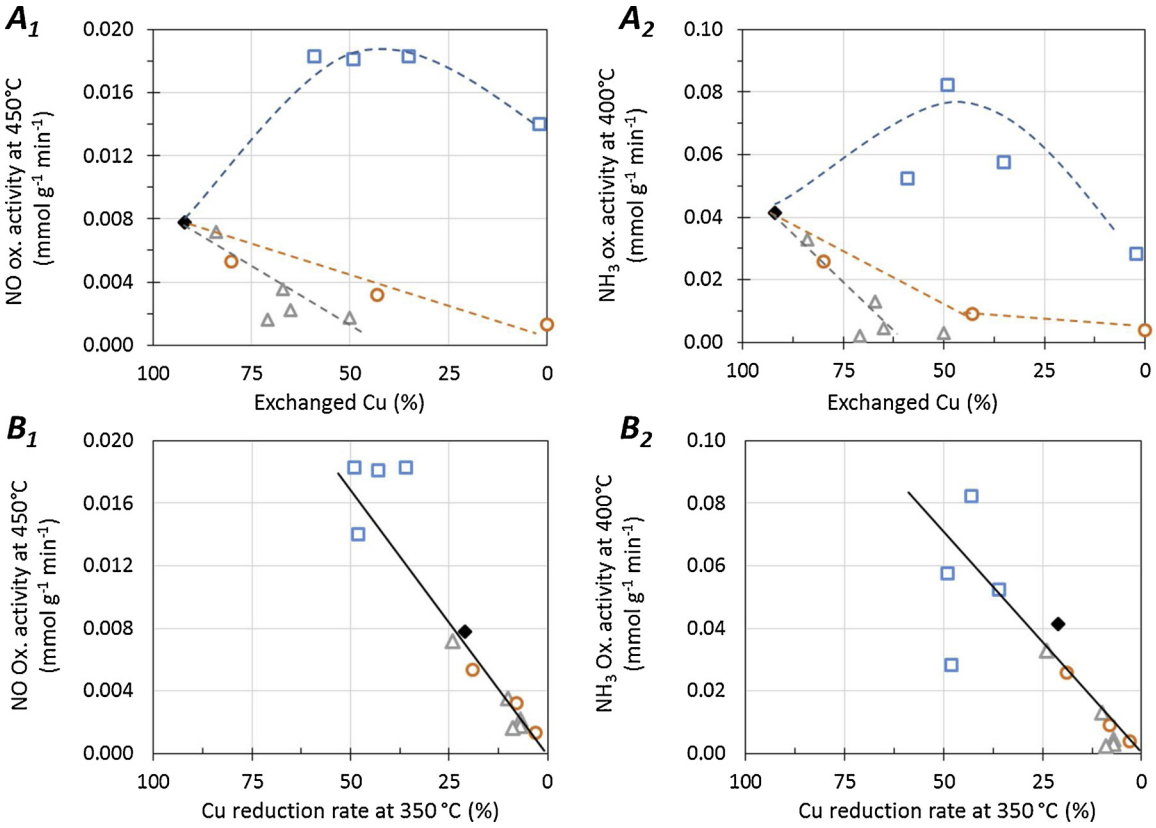

Fig. 11. Effect of catalysts characteristics (exchanged Cu^{2+} ratio (A); copper reduction rate at 350 °C from TPR profiles (B)) on NO and NH_3 oxidation activity. (◆: Cu/FER; □, —: Cu/FER@(Na); △, —: Cu/FER@(P); ○, —: Cu/FER@(Na + P)).

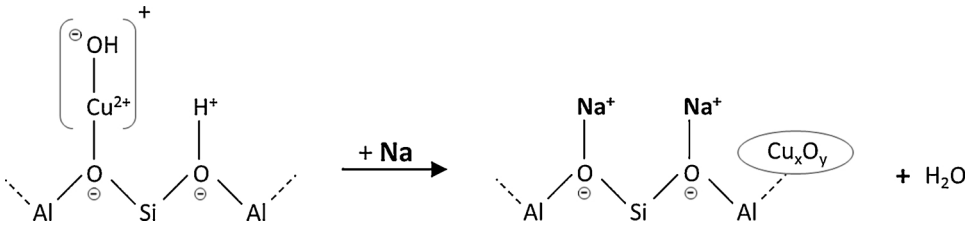

Scheme 1. Schematic illustration of the impact of sodium addition on Cu/FER catalyst.

unit is more significant in presence of phosphorus.

However, the Cu-P interaction is clearly the driving force for the catalyst deactivation in NO and NH_3 oxidation reactions (Fig. 11-B). As a result, the simultaneous addition of both inorganic compounds did not lead to an additive effect of deactivation. Scheme 3 illustrates the combination of the (Na + P) co-addition, with the formation of external CuO by Cu^{2+}-Na^+ back-exchange and the copper-phosphorus interactions considering metaphosphate ion.

Finally, the addition of mineral compounds over Cu-FER strongly altered both acid and redox sites, with variable pathways depending on the considered inorganic element. The next section aims to highlight the poisoning effects of each Na and/or P addition on the DeNOx efficiency.

3.4.2. *Relationships between the poisoning effects and the DeNOx efficiency*

To highlight a general overview of the catalyst deactivation generated by inorganic elements, various possible correlations were investigated. Figs. 12 and 13 report the obtained relationships between catalytic activities in NH_3-SCR at selected temperatures of 250 °C and 500 °C and surface properties characterized by means of NH_3 adsorption capacity, NO oxidation behavior and H_2-TPR experiments. Deactivations in both standard and fast-SCR conditions are examined.

At low temperature (250 °C), NH_3-SCR performances appeared directly correlated with the NH_3 sorption properties, whatever the considered catalysts (Fig. 12-A). It means that ammonia adsorption is a key parameter in the NH_3 SCR reaction pathway, as reported in [37]. Interestingly, this relationship did not depend on the involved ammonia adsorption sites, either Brønsted sites or copper sites because the poisoning of NH_3 adsorption sites was different in function of the considered inorganic element. Sodium addition was showed to neutralize the acid sites and favored the exchanged Cu^{2+} migration to form CuO compounds, leading to a loss in accessible copper sites (Scheme 1). For only phosphorus containing catalysts, exchanged Cu^{2+} sites were poisoned by P (Scheme 2), with limited impact on exchanged Cu^{2+} migration to form CuO compounds (Fig. 3). Both Na and P effects were observed after (Na + P) co-addition. Note also that the relationship between the SCR activity and the NH_3 sorption properties was not dependent on the inlet NO_2/NOx ratio because this correlation was obtained in both standard and fast SCR stoichiometry. In other words, the NO oxidation rate poisoning is not the main parameter for SCR deactivation. Nevertheless, the redox function poisoning by phosphorus addition also appeared to drive the SCR activity at 250 °C, as highlighted by the correlation illustrated in Fig. 12-B.

At higher temperature (500 °C), the SCR efficiency was actually connected to the amount of exchanged Cu^{2+} species for sodium only containing catalyst (Fig. 13). It is concluded that the migration of

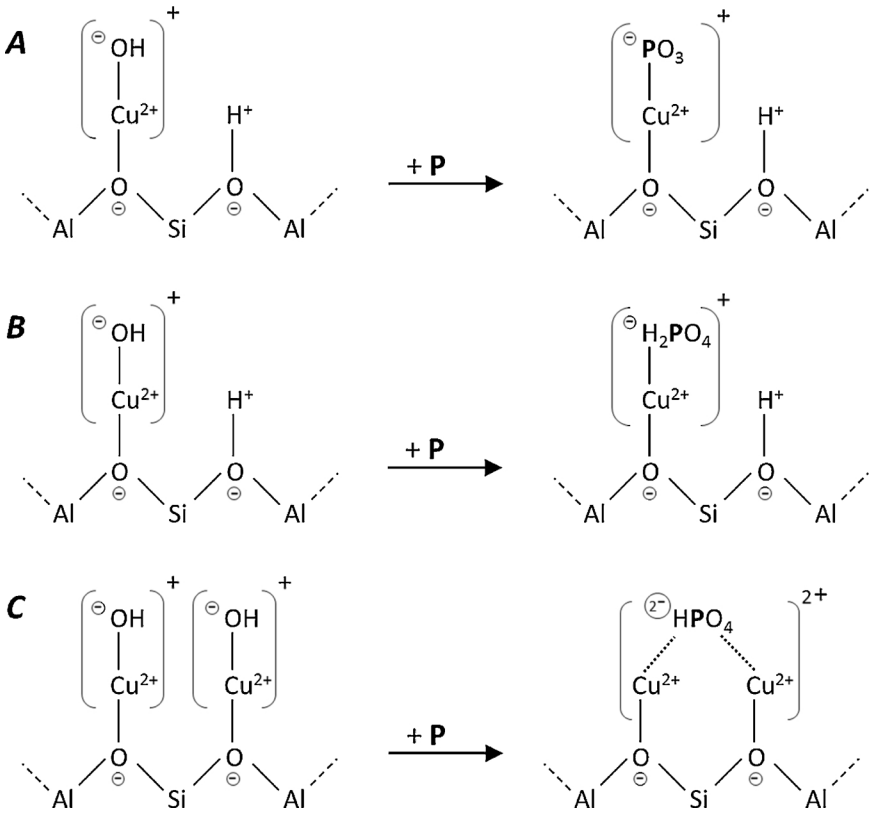

Scheme 2. Schematic illustration of the impact of phosphorus addition on Cu/FER catalyst, considering the formation of (A): metaphosphate, (B): dihydrogen phosphate and (C): hydrogen phosphate.

exchanged Cu^{2+} species at the expense of the CuO formation induced an over-consumption of NH_3 with a detrimental effect on the SCR function at 500 °C. This result was in accordance with the improvement in the NH_3 and NO oxidation behaviors with the CuO formation. Phosphorus addition or co-addition of (Na + P) negatively affected the ammonia oxidation behaviour, and consequently inhibited the competition between NH_3 oxidation and SCR at high temperature. No correlation was obtained for P containing materials, only Na single addition significantly poisoned SCR performances at high temperature.

Finally, the observed relationships between the poison-catalyst interactions and the catalytic behaviors differed considering the oxidation reaction or the DeNOx efficiency. Clearly, the redox function, linked with the copper condition, is the main driving force for the oxidation reactions. For the NH_3-SCR process, the ammonia adsorption ability, which depends on both acidity and copper state, appeared the main key parameter.

4. Conclusion

This work aimed to highlight the deactivation mechanisms encountered by minerals impurities from Biodiesel over a model Cu-FER catalyst dedicated to NH_3-SCR. It was evidenced that sodium and phosphorus interacted differently with the catalyst. Na addition induced a loss of Brønsted acid sites and a back-exchange of Cu^{2+} with Na^+ (probably during the impregnation step), with formation of external CuO species favoring the oxidation reactions of NO and NH_3. On the contrary, the exchanged Cu^{2+} species remained moderately affected by phosphorus addition, but direct interactions with copper were evidenced, which were responsible for catalyst deactivation toward the oxidation reactions. After equimolar addition of phosphorus and sodium, both Na and P interact with the catalyst. Clearly, the redox function, linked with the copper condition, was evidenced to be the main driving force for the oxidation reactions. However, high NH_3 oxidation activity is detrimental for the DeNOx efficiency at high temperature (500 °C) due to the reductant consumption. At low temperature (250 °C), the DeNOx efficiency was mainly correlated with the NH_3 adsorption capacities, which depends on both acidity and copper state. Then, phosphorus appeared to be the major responsible for catalyst deactivation after (Na + P) co-poisoning.

Acknowledgments

The authors gratefully acknowledge the French Agence Nationale de la Recherche (ANR, Appibio Project, ref. ANR-14-CE22-0003), the European Regional Development Fund (FEDER) and the "Région Nouvelle Aquitaine" for the financial supports.

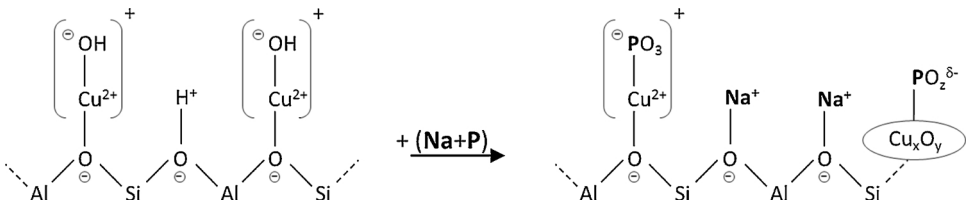

Scheme 3. Schematic illustration of the impact of both sodium and phosphorus addition on Cu/FER catalyst.

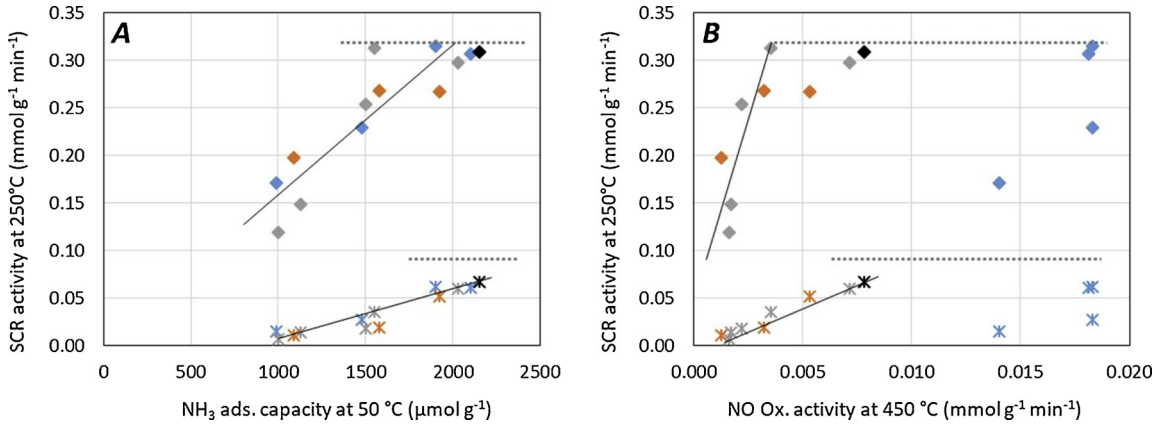

Fig. 12. Relationship between standard (⚹) or fast (♦) SCR activities (mmol g^{-1} min^{-1}) at 250 °C in function of (A) NH_3 adsorption capacities at 50 °C (µmol g^{-1}) and (B) NO oxidation activities at 450 °C. (⚹,♦): Cu/FER; (⚹,♦): Cu/FER@(Na); (⚹, ◆): Cu/FER@(P); (⚹, ◆): Cu/FER@(Na + P). In dotted line is presented the activity for 100% NOx conversion in NH_3-SCR.

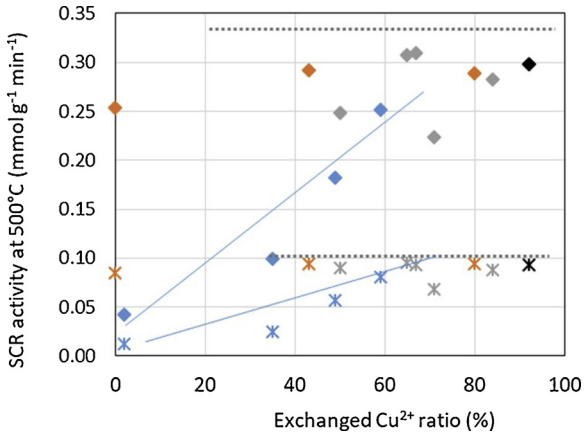

Fig. 13. Relationship between standard (⚹) and fast (♦) SCR activities (mmol/g/min) at 500 °C in function of exchanged Cu^{2+} ratio (%). (⚹,♦): Cu/FER; (⚹,♦): Cu/FER@(Na); (⚹, ◆): Cu/FER@(P); (⚹, ◆): Cu/FER@(Na + P).). In dotted line is presented the activity for 100% NOx conversion in NH_3-SCR.

References

[1] C. Paolucci, J.R. Di Iorio, F.H. Ribeiro, R. Gounder, W.F. Schneider, Chapter one – catalysis science of NOx selective catalytic reduction with ammonia over Cu-SSZ-13 and Cu-SAPO-34, J. Adv. Catal. Sci. Technol. 59 (2016) 1–107.

[2] F.X. Llabrés i Xamena, P. Fisicaro, G. Berlier, A. Zecchina, G. Turnes Palomino, C. Prestipino, S. Bordiga, E. Giamello, C.J. Lamberti, Thermal reduction of Cu^{2+} – mordenite and re-oxidation upon interaction with H_2O, O_2, and NO, J. Phys. Chem. B 107 (2003) 7036–7044.

[3] F. Gao, N.M. Washton, Y. Wang, M. Kollár, J. Szanyi, C.H.F. Peden, Effects of Si/Al ratio on Cu-SSZ-13 NH_3-SCR catalysts: implications for the active Cu species and the roles of Brønsted acidity, J. Catal. 331 (2015) 25–38.

[4] J. Dědeček, B. Wichterlová, Role of hydrated Cu ion complexes and aluminum distribution in the framework on the Cu ion siting in ZSM-5, J. Phys. Chem. B 101 (1997) 10233–10240.

[5] P.D. Costa, B. Modén, G.D. Meitzner, D.K. Lee, E. Iglesia, Spectroscopic and chemical characterization of active and inactive Cu species in NO decomposition catalysts based on Cu-ZSM5, Phys. Chem. Chem. Phys. 4 (2002) 4590–4601.

[6] T.V.W. Janssens, H. Falsig, L.F. Lundegaard, P.N.R. Vennestrøm, S.B. Rasmussen, P.G. Moses, F. Giordanino, E. Borfecchia, K.A. Lomachenko, C. Lamberti, S. Bordiga, A. Godiksen, S. Mossin, P. Beato, A consistent reaction scheme for the selective catalytic reduction of nitrogen oxides with ammonia, ACS Catal. 5 (2015) 2832–2845.

[7] R.P. Ruggeri, I. Nova, E. Tronconi, Experimental study of the NO oxidation to NO_2 over metal promoted zeolites aimed at the identification of the standard SCR rate determining step, Top. Catal. 56 (2013) 109–113.

[8] E. Iojoiu, V. Lauga, J. Abboud, G. Legros, J. Bonnety, P. Da Costa, J. Schobing, A. Brillard, G. Leyssens, V. Tschamber, P. Anguita, J.G. Vargas, L. Retailleau, S. Gil, A. Giroir-Fendler, M.-L. Tarot, F. Can, D. Duprez, X. Courtois, Biofuel impact on diesel engine after-treatment: deactivation mechanisms and soot reactivity, Emiss. Control. Sci. Technol. 4 (1) (2017) 15–32.

[9] S. Shwan, J. Jansson, L. Olsson, M. Skoglundh, Chemical deactivation of Fe-BEA as NH_3-SCR catalyst—effect of phosphorous, Appl. Catal. B Environ. 147 (2014) 111–123.

[10] S. Andonova, E. Vovk, J. Sjöblom, E. Ozensoy, L. Olsson, Chemical deactivation by phosphorous under lean hydrothermal conditions over Cu-BEA NH_3-SCR catalysts, Appl. Catal. B Environ. 147 (2014) 251–263.

[11] K. Xie, K. Leistner, K. Wijayanti, A. Kumar, K. Kamasamudram, L. Olsson, Influence of phosphorus on Cu-SSZ-13 for selective catalytic reduction of NOx by ammonia, Catal. Today 297 (2017) 46–52.

[12] P. Kern, M. Klimczak, T. Heinzelmann, M. Lucas, P. Claus, High-throughput study of the effects of inorganic additives and poisons on NH_3-SCR catalysts. Part II: Fe–zeolite catalysts, Appl. Catal. B Environ. 95 (2010) 48–56.

[13] S. Shwan, J. Jansson, L. Olsson, M. Skoglundh, Chemical deactivation of H-BEA and Fe-BEA as NH_3-SCR catalysts—effect of potassium, Appl. Catal. B Environ. 166–167 (2015) 277–286.

[14] J. Ma, Z. Si, D. Weng, X. Wu, Y. Ma, Potassium poisoning on Cu-SAPO-34 catalyst for selective catalytic reduction of NOx with ammonia, Chem. Eng. J. 267 (2015) 191–200.

[15] Z. Zhao, R. Yu, R. Zhao, C. Shi, H. Gies, F.S. Xiao, D. De Vos, T. Yokoi, X. Bao, U. Kolb, M. Feyen, R. McGuire, S. Maurer, A. Moini, U. Muller, W. Zhang, Cu-exchanged Al-rich SSZ-13 zeolite from organotemplate-free synthesis as NH_3-SCR catalyst: effects of Na+ ions on the activity and hydrothermal stability, Appl. Catal. B 217 (2017) 421–428.

[16] M.-L. Tarot, M. Barreau, D. Duprez, V. Lauga, E.-E. Iojoiu, X. Courtois, F. Can, Influence of the sodium impregnation solvent on the deactivation of Cu-FER-exchanged zeolites dedicated to the SCR of NOx with NH_3, Catalysts 8 (2018) 3–20.

[17] M. Ajmal, A. Hussain Khan, S. Ahmad, A. Ahmad, Role of sawdust in the removal of copper(II) from industrial wastes, Water Res. 32 (1998) 3085–3091.

[18] M. Trombetta, G. Busca, S. Rossini, V. Piccoli, U. Cornaro, A. Guercio, R. Catani, R.J. Willey, FT-IR studies on light olefin skeletal isomerization catalysis: III. Surface acidity and activity of amorphous and crystalline catalysts belonging to the SiO_2–Al_2O_3 system, J. Catal. 179 (1998) 581–596.

[19] B. Wichterlová, Z. Tvarůžková, Z. Sobalík, P. Sarv, Determination and properties of acid sites in H-ferrierite: a comparison of ferrierite and MFI structures, Microporous Mesoporous Mater. 24 (1998) 223–233.

[20] M. Moreno-Gonzalez, B. Hueso, M. Boronat, T. Blasco, A. Corma, Ammonia-containing species formed in Cu-Chabazite as per in situ EPR, solid-state NMR and DFT calculations, J. Phys. Chem. Lett. 6 (2015) 1011–1017.

[21] A. Delabie, K. Pierloot, M.H. Groothaert, B.M. Weckhuysen, R.A. Schoonheydt, Study of the coordination of Cu^{2+} in zeolite Y: interaction with water and ammonia, Microporous Mesoporous Mater. 37 (2000) 209–222.

[22] R. Bulánek, B. Wichterlová, Z. Sobalík, J. Tichý, Reducibility and oxidation activity of Cu ions in zeolites: effect of Cu ion coordination and zeolite framework composition, Appl. Catal. B Environ. 31 (2001) 13–25.

[23] G. Delahay, B. Coq, L. Broussous, Selective catalytic reduction of nitrogen monoxide by decane on copper-exchanged beta zeolites, Appl. Catal. B Environ. 12 (1997) 49–59.

[24] J.M. Dumas, C. Geron, A. Kribii, J. Barbier, Preparation of supported copper catalysts, Appl. Catal. B Environ. 47 (1989) 9–15.

[25] J. Luo, F. Gao, K. Kamasamudram, N. Currier, C.H.F. Peden, A. Yezerets, New insights into Cu-SSZ-13 SCR catalyst acidity. Part I: nature of acidic sites probed by NH3 titration, J. Catal. 348 (2017) 291–299.

[26] C. Torre-Abreu, M.F. Ribeiro, C. Henriques, G. Delahay, NO TPD and H_2-TPR studies for characterisation of CuMOR catalysts. The role of Si/Al ratio, copper content and cocation, Appl. Catal. B Environ. 14 (1997) 261–272.

[27] C. Sepúlveda, L. Delgado, R. García, M. Melendrez, J.L.G. Fierro, I.T. Ghampson, N. Escalona, Effect of phosphorous on the activity of Cu-SiO_2 catalysts in the hydrogenolysis of glycerol, Catal. Today 279 (2017) 217–223.

[28] G.V. Mamontov, O.V. Magaev, A.S. Knyazev, O.V. Vodyankina, Influence of phosphate addition on activity of Ag and Cu catalysts for partial oxidation of alcohols, Catal. Today 203 (2013) 122–126.

[29] A. Asha Radhakrishnan, B. Baskaran Beena, Structural and optical absorption analysis of CuO nanoparticles, Indian J. Adv. Chem. Sci. 2 (2) (2014) 158–161.
[30] R.P. Ye, L. Lin, C.C. Chen, J.X. Yang, F. Li, X. Zhang, D.J. Li, Y.Y. Qin, Z. Zhou, Y.G. Yao, Synthesis of robust MOF-derived Cu-SiO2 catalyst with low copper loading via sol-gel method for the dimethyl oxalate hydrogenation reaction, ACS Catal. 8 (4) (2018) 3382–3394.
[31] G. Müller, J. Bódis, G. Eder-Mirth, J. Kornatowski, J.A. Lercher, In situ FT-IR microscopic investigation of metal substituted $AlPO_4$-5 single crystals, J. Mol. Struct. 410-411 (1997) 173–178.
[32] D. Wang, L. Zhang, J. Li, K. Kamasamudram, W.S. Epling, NH_3-SCR over Cu-SAPO-34 – zeolite acidity and Cu structure changes as a function of Cu loading, Catal. Today 231 (2014) 64–74.
[33] F. Gao, D.H. Mei, Y.L. Wang, J. Szanyi, C.H.F. Peden, Selective catalytic reduction over Cu/SSZ-13: linking homo- and heterogeneous catalysis, J. Am. Chem. Soc. 139 (2017) 4935–4942.
[34] C. Paolucci, I. Khurana, A.A. Parekh, S.C. Li, A.J. Shih, H. Li, J.R. Di Iorio, J.D. Albarracin-Caballero, A. Yezerets, J.T. Miller, W.N. Delgass, F.H. Ribeiro, W.F. Schneider, R. Gounder, Dynamic multinuclear sites formed by mobilized copper ions in NOx selective catalytic reduction, Science 357 (2017) 898–903.
[35] A. Grossale, I. Nova, E. Tronconi, D. Chatterjee, M. Weibel, The chemistry of the NO/NO_2–NH_3 “fast” SCR reaction over Fe-ZSM5 investigated by transient reaction analysis, J. Catal. 256 (2008) 312–322.
[36] M.L. Tarot, V. Lauga, E.E. Iojoiu, X. Courtois, F. Can, Influence of sodium and/or phosphorus addition on the deactivation of Cu-FER zeolites for SCR of NOx with NH_3, Top. Catal. 62 (1-4) (2019) 72–78.
[37] T. Yu, T. Hao, D. Fan, J. Wang, M. Shen, W. Li, Recent NH_3-SCR mechanism research over Cu/SAPO-34 catalyst, J. Phys. Chem. C 118 (2014) 6565–6575.